Hindawi
Complexity
Volume 2022, Article ID 7634357, 20 pages
https://doi.org/10.1155/2022/7634357

Research Article

Consequence of Double-Diffusion Convection and Partial Slip on Magneto-Oldroyd-4 Constants Nanofluids with Peristaltic Propulsion in an Asymmetric Channel

Maria Athar,[1] **Yasir Khan**,[2] **Safia Akram**,[3] **Khalid Saeed**,[4] **A. Alameer**,[2] **and Anwar Hussain**[5]

[1]*National University of Modern Languages, Islamabad, Pakistan*
[2]*Department of Mathematics, University of Hafr Al-Batin, Hafr Al-Batin 31991, Saudi Arabia*
[3]*MCS, National University of Sciences and Technology, Islamabad, Pakistan*
[4]*Comsats University, Islamabad, Pakistan*
[5]*Department of Mechanical Engineering, School of Mechanical and Manufacturing Engineering, National University of Sciences and Technology, Islamabad, Pakistan*

Correspondence should be addressed to Safia Akram; drsafiaakram@gmail.com

Received 25 July 2022; Accepted 13 September 2022; Published 30 September 2022

Academic Editor: Lingzhong Guo

The double-diffusive convection is a significant physical phenomenon that arises in fluid mechanics. It is primarily associated with a convection process in which two dissimilar density gradients with varying diffusion rates are considered. The primary goal of this study is to investigate the effects of double-diffusivity convection and partial slip with an inclined magnetic field on peristaltic propulsion in an asymmetric channel for Oldroyd-4 constants nanofluids. The flow of an Oldroyd-4 constant nanofluid is mathematically modeled in the presence of double-diffusivity convection and a tilted magnetic field. Lubrication methodology is applied to simplify the highly nonlinear system of partial differential equations (PDEs). The numerical scheme is used to calculate the solution of coupled nonlinear PDEs. Furthermore, the effect of changing the parameters associated with slip, thermophoresis, Brownian motion, Grashof number of nanoparticles, Hartmann number, pumping, and trapping are investigated in this article. It is noticed that the temperature rises as the Brownian motion and thermophoresis constraints increases. This is because the growth in the Brownian motion parameter indicates the increase in the kinetic energy of nanoparticles which results in warming up the nanofluid. Also, concentration falls as the Brownian motion and thermophoresis constraints increases.

1. Introduction

The peristaltic transportation of biological fluids has huge number of applications in biomedical industry and hence received huge attention from the researchers in last two decades. Transport phenomenon of biological fluids is based on peristaltic propulsion. This phenomenon can be internally observed in the gastrointestinal tract, urine flow, blood flow, male reproductive tract, esophageal swallowing, and ureter and externally as worm's movement. This natural process is caused by periodic relaxation and contraction of muscles which produce a sinusoidal wave along the channel or tube walls. Some of the worthwhile theoretical and experimental studies considering the peristaltic propulsion for numerous basic fluid models are cited in references [1–6]. These studies have further been generalized for many non-Newtonian fluid models like the Carreau model [7], Maxwell model [8], Johnson–Segalman model [9], Williamson model [10], Casson model [11], six-constant Jeffreys model [12], Walter's B model [13], hyperbolic tangent model [14], Herschel–Bulkley model [15], Jeffrey model [16], Sisko fluid [17], Oldroyd-4 model [18], Phan–Thien–Tanner model [19], and Burgers' model [20]. The authors of these research studies extended the work to new findings which may widen the horizon of their usage to biomedical engineering and technology.

In the field of biomagnetic fluid dynamics (BFD), the study of peristaltic flow is based on magnetohydrodynamic (MHD) effects. The study of these biological fluids (examples of biofluids include blood, urine, and chyme) flows is important in bioengineering and medical sciences. These fluids are broadly found in living organisms and influence of magnetic field effects the flow greatly. Also, in peristaltic MHD compressor and blood pump machines, MHD effects on conductive physiological fluids become vital [21–25].

Nanotechnology is considered important in improving as well as revolutionizing information technology, industry sectors, homeland security, energy, food safety, medicine, transportation, and environmental discipline. In this century, many researchers and mathematicians are working on the development of mathematics and physics of nanofluid mechanics. This is due to the fact that nanotechnology is used in industry to get the optimum outputs in constrained environment. It is, therefore, an attractive research area in the modern fluid mechanics. Nanofluids are composed by dissemination of nanosized materials/particles in the base fluids (both viscous and inviscid liquids). It is known that the term nanofluid was introduced first ever by J. C. Maxwell, a Scottish scientist, in the late nineteenth century. Mostly, modern work is based on the analysis of nanofluids made by the Choi [26]. From this productive study, a vast number of applications of nanotechnology can be found in microchannel cooling and reduction/enhancement in heat transfer. The bond of peristalsis with nanofluids has many utilizations in biomedical science (e.g., radiotherapy for cancer cure and drug delivery), chemical, and mechanical engineering (pumps and transportation of chemicals). Recently, such studies of nanoparticles along with different flow geometries have been examined extensively in physiological flows, such as references [27–35].

The double-diffusive convection is an important physical phenomenon arising in fluid mechanics. It is mainly associated with such a convection process where two dissimilar density gradients, having a diverse diffusion rate, are considered. The literature review tells us that none of the analysis has been considered for the double diffusion convection with assumptions of creeping phenomena and low Reynolds number. The double diffusion convection and peristaltic pumping have many applications of the innate mechanism in industrial and chemical engineering. Because of these applications, some authors have contributed to this area with various fluid models. Few are cited in references [36–42].

Incorporation of partial slips in fluid flows is essential in the study of polymers and polishing the artificial heart valve. To the best of our knowledge, the slip effects were first used in the peristalsis by Chu and Fang [43]. Later, Akbar et al. [44] further added these effects to examine the influence on peristaltic flow of nanofluid. Also, these effects on hydromagnetic driven peristaltic flow were investigated by Abbasi et al. in reference [45]. More recent works on these effects can be viewed in references [46–50].

From the abovementioned discussion, the heat convection impact and magnetic flux on double diffusion convection cannot be neglected. The study of the Oldroyd-4 constant nanofluid is studied in the literature but effects of double diffusion and partial slip with inclined MHD are not studied yet. So, the rationale of our current research is to show how magnetic field and slip boundaries affect peristaltic flow and heat transfer with double diffusion convection.

2. Flow Equations

The equations that describe flow in an incompressible fluid are as follows [36, 37]:

$$
\begin{aligned}
&\operatorname{div} V = 0,\\
&\rho_f\left(\frac{dV}{dt}\right) = \operatorname{div}\tau + \rho f + g\left\{(1-\Theta_0)\rho_{f0}\beta_T(T-T_0)\right.\\
&\qquad + \beta_C(C-C_0)\\
&\qquad \left.-\left(\rho_p-\rho_{f0}\right)(\Theta-\Theta_0)\right\},\\
&(\rho c)_f\left(\frac{dT}{dt}\right) = k\nabla^2 T + (\rho c)_p\{D_B(\nabla\Theta\cdot\nabla T)\\
&\qquad +\left(\frac{D_T}{T_0}\right)\nabla T\cdot\nabla T\} + D_{TC}\nabla^2 C,\\
&\frac{dC}{dt} = D_s\nabla^2 C + D_{TC}\nabla^2 T,\\
&\frac{d\Theta}{dt} = D_B\nabla^2\Theta + \left(\frac{D_T}{T_0}\right)\nabla^2 T.
\end{aligned}
\tag{1}
$$

In the abovementioned equations, temperature is represented by T, concentration, by C, nanoparticle volume fraction, by Θ, V represents velocity, d/dt illustrates material time derivative, f stands for body force, τ describes stress tensor, g is acceleration, ρ_f represents base fluid density, particles density is represented ρ_p, ρ_{f_0} describes fluid density at T_0, $(\rho c)_p$ denotes the thermal capacity of nanoparticles, $(\rho c)_f$ refers fluid heat capacity, β_T describes fluid volumetrical thermal expansion coefficient, β_C stands for fluid volumetrical solutal expansion coefficient, D_{TC} denotes Dufour diffusively, Soret diffusively is denoted by D_{CT}, D_B is coefficient of Brownian diffusion, D_T coefficient of thermophoretic diffusion, D_s stands for solutal diffusively, and thermal conductivity is represented by k.

The Oldroyd-4 constant fluid stress tensor in [18] is defined by the following equations:

$$\tau = -PI + S,$$
$$S + \lambda_1 \frac{DS}{Dt} + \lambda_3 tr(S) A_1 = \mu\left(1 + \lambda_2 \frac{D}{Dt}\right) A_1,$$
$$A_1 = (\nabla V) + (\nabla V)^*, \tag{2}$$
$$\frac{DS}{Dt} = \frac{dS}{dt} - (\nabla V) S - S (\nabla V)^*.$$

Where (λ_1, λ_3) represents relaxation times, λ_2 is retardation time, μ is denoted by viscosity, $*$ is used for transpose, and A_1 is Rivilin–Ericksen tensors.

3. Mathematical Formulation

We assume that an incompressible peristaltic flow and electrically conducting of Oldroyd-4 constant nanofluid in 2 dimensional conduit having width equal to $d_1 + d_2$, in the Cartesian coordinates system. The channel's center is supposed to be along horizontal line, and cross-sectional area is assumed to be beside the vertical line. Conduit boundary is assumed to be moving with constant speed and shape like sinusoidal wave train. Temperatures, solvent concentrations, and nanoparticle concentrations of the lower and upper walls are (T_1, T_0), $(C_1 C_0)$, and $(\Theta_1 \Theta_0)$, respectively. Fixed magnetic field at an angle β is applied on the flow. It is assumed that electric field is zero and the Reynolds number is low so that it produces insignificant induced magnetic field as compared to applied magnetic field.

The geometric shape of wall is specified in Figure 1 and mathematical expression is defined as follows[3]:

$$H_1 = Y = d_1 + d_3 \cos\left[\frac{2\pi}{\lambda}(X - ct)\right],$$
$$H_2 = Y = -d_2 - d_4 \cos\left[\frac{2\pi}{\lambda}(X - ct) + \varphi\right], \tag{3}$$

where $(d_3 d_4)$ illustrates wave amplitudes, $d_1 + d_2$ is channel width, λ illustrates wavelength, t indicates time, and c is wave velocity. The range of phase difference (φ) is $0 \le \varphi \le \pi$. When $\varphi = 0$, the channel is symmetric without a phase wave and at $\varphi = \pi$, the channel with a phase wave. Furthermore, the constraints φ, d_1, d_2, d_3, and d_4 satisfy the condition $d_3^2 + d_4^2 + 2 d_3 d_4 \cos\varphi \le (d_1 + d_2)^2$ The velocity field in 2− directional and dimensional flow is. $V = (U(X, Y, t))$, $V(X, Y, t), 0)$

The motion equations in 2− dimensional incompressible flow comprising Oldroyd-4 constant nanofluid are as follows:

$$\frac{\partial U}{\partial X} + \frac{\partial V}{\partial Y} = 0, \tag{4}$$

$$\begin{aligned}\rho_f\left(\frac{\partial}{\partial t} + U\frac{\partial}{\partial X} + V\frac{\partial}{\partial Y}\right)U = &-\frac{\partial P}{\partial X} + \frac{\partial}{\partial X}(S_{XX}) + \frac{\partial}{\partial Y}(S_{XY}) - \sigma B_0^2 \cos\beta (U\cos\beta - V\sin\beta)\\ &+ g\left\{(1 - \Theta_0)\rho_{f0}\{\beta_T (T - T_0) + \beta_C (C - C_0)\} - \left(\rho_p - \rho_{f0}\right)(\Theta - \Theta_0)\right\},\end{aligned} \tag{5}$$

$$\begin{aligned}\rho_f\left(\frac{\partial}{\partial t} + U\frac{\partial}{\partial X} + V\frac{\partial}{\partial Y}\right)V = &-\frac{\partial P}{\partial Y} + \frac{\partial}{\partial X}(S_{YX}) + \frac{\partial}{\partial Y}(S_{YY})\\ &+ \sigma B_0^2 \sin\beta (U\cos\beta - V\sin\beta),\end{aligned} \tag{6}$$

$$\begin{aligned}(\rho c)_f\left(\frac{\partial}{\partial t} + U\frac{\partial}{\partial X} + V\frac{\partial}{\partial Y}\right)T = k\left(\frac{\partial^2 T}{\partial X^2} + \frac{\partial^2 T}{\partial Y^2}\right) + (\rho c)_p\Bigg\{D_B\left(\frac{\partial \Theta}{\partial X}\frac{\partial T}{\partial X} + \frac{\partial \Theta}{\partial Y}\frac{\partial T}{\partial Y}\right)\\ \left(\frac{D_T}{T_0}\right)\left[\left(\frac{\partial T}{\partial X}\right)^2 + \left(\frac{\partial T}{\partial Y}\right)^2\right]\Bigg\} + D_{TC}\left(\frac{\partial^2 C}{\partial X^2} + \frac{\partial^2 C}{\partial Y^2}\right),\end{aligned} \tag{7}$$

$$\left(\frac{\partial}{\partial t} + U\frac{\partial}{\partial X} + V\frac{\partial}{\partial Y}\right)C = D_s\left(\frac{\partial^2 C}{\partial X^2} + \frac{\partial^2 C}{\partial Y^2}\right) + D_{TC}\left(\frac{\partial^2 T}{\partial X^2} + \frac{\partial^2 T}{\partial Y^2}\right), \tag{8}$$

$$\left(\frac{\partial}{\partial t} + U\frac{\partial}{\partial X} + V\frac{\partial}{\partial Y}\right)\Theta = D_B\left(\frac{\partial^2 \Theta}{\partial X^2} + \frac{\partial^2 \Theta}{\partial Y^2}\right) + \left(\frac{D_T}{T_0}\right)\left(\frac{\partial^2 T}{\partial X^2} + \frac{\partial^2 T}{\partial Y^2}\right). \tag{9}$$

Using the Galilean transformation between fixed and wave frames as follows:

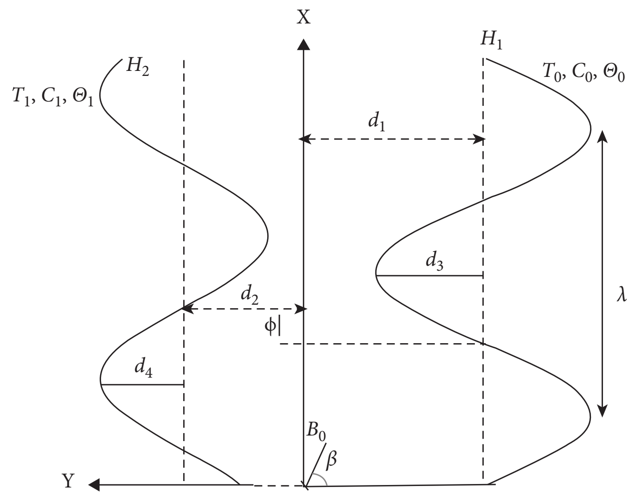

Figure 1: Geometry of the problem.

$$\begin{aligned} v &= V, \\ y &= Y, \\ u &= U - c, \\ x &= X - ct, \\ p(x, y) &= P(X, Y, t), \end{aligned} \tag{10}$$

Defining the dimensionless quantities as follows:

$$\begin{aligned} &\bar{x} = \frac{x}{\lambda}, \bar{u} = \frac{u}{c}, \bar{y} = \frac{y}{d_1}, \bar{v} = \frac{v}{c}, \delta = \frac{d_1}{\lambda}, d = \frac{d_2}{d_1}, \bar{t} = \frac{ct}{\lambda}, h_2 = \frac{H_2}{d_2}, h_1 = \frac{H_1}{d_1}, b = \frac{d_4}{d_1}, \bar{p} = \frac{d_1^2 p}{\mu c \lambda}, \\ &a = \frac{d_3}{d_1}, Pr = \frac{(\rho c)_f \upsilon}{k}, \mathrm{Re} = \frac{\rho_f c d_1}{\mu}, \upsilon = \frac{\mu}{\rho_f}, Le = \frac{\upsilon}{D_s}, Ln = \frac{\upsilon}{D_B}, u = \frac{\partial \psi}{\partial y}, v = -\delta \frac{\partial \psi}{\partial x}, \\ &M = \sqrt{\frac{\sigma}{\mu}} B_0 d_1, \theta = \frac{T - T_0}{T_1 - T_0}, \gamma = \frac{C - C_0}{C_1 - C_0}, \bar{\lambda}_2 = \frac{\lambda_2 c}{d_1}, \bar{\lambda}_3 = \frac{\lambda_3 c}{d_1}, \bar{S} = \frac{\mu c}{d_1} S, N_{TC} = \frac{D_{CT}(C_1 - C_0)}{k(T_1 - T_0)}, \\ &G_{rt} = \frac{g d_1^2 (1 - \Theta_0)(T_1 - T_0)\rho_f \beta_T}{\mu c}, G_{rc} = \frac{g(1 - \Theta_0)\rho_f \beta_c (C_1 - C_0) d_1^2}{\mu c}, \Omega = \frac{\Theta - \Theta_0}{\Theta_1 - \Theta_0}, \bar{\lambda}_1 = \frac{\lambda_1 c}{d_1}, \\ &G_{rF} = \frac{g(\rho_p - \rho_f)(\Theta_1 - \Theta_0)}{\mu c} d_1^2, N_t = \frac{(\rho c)_p D_T (T_1 - T_0)}{T_0 k}, N_b = \frac{(\rho c)_p D_B (\Theta_1 - \Theta_0)}{k}, \\ &N_{CT} = \frac{D_{CT}(T_1 - T_0)}{(C_1 - C_0) D_s}. \end{aligned} \tag{11}$$

Where G_{rt}, $Re G_{rF} N_{CT} G_{rc} Pr N_{TC} \gamma M N_t \Omega, Le, \theta, N_b, Ln$, and δ stands for thermal Grashof number, Reynolds number, nanoparticle Grashof number, Soret parameter, solutal Grashof number, Prandtl number, Dufour parameter, solutal (species) concentration, Hartmann number, thermophoresis parameter, nanoparticle fraction, Lewis number, temperature, Brownian motion, Lewis number of nanofluid, and wave number, respectively.

Now, using (10) and (11), (4) is identically satisfied and equations (12)–(16) (after omitting bars) in the wave frame becomes as follows:

$$\begin{aligned}\mathrm{Re}\delta\left(\Psi_y\Psi_{xy}-\Psi_x\Psi_{yy}\right) &= -\frac{\partial p}{\partial x}+\delta\frac{\partial S_{xx}}{\partial x}+\frac{\partial S_{xy}}{\partial y}\\ &\quad - M^2\cos\beta\left(\left(\Psi_y+1\right)\cos\beta+\Psi_x\delta\sin\beta\right)\\ &\quad + G_{rt}\theta+G_{rc}\gamma-G_{rF}\Omega,\end{aligned} \tag{12}$$

$$\begin{aligned}\mathrm{Re}\delta^3\left(\Psi_x\Psi_{xy}-\Psi_y\Psi_{xx}\right) &= -\frac{\partial p}{\partial y}+\delta^2\frac{\partial S_{yx}}{\partial x}+\delta\frac{\partial S_{yy}}{\partial y}\\ &\quad + M^2\delta\sin\beta\left(\left(\Psi_y+1\right)\cos\beta\right.\\ &\quad \left.+\Psi_x\delta\sin\beta\right),\end{aligned} \tag{13}$$

$$\begin{aligned}\mathrm{Re}Pr\delta\left(\Psi_y\theta_x-\Psi_x\theta_y\right) &= \left(\theta_{yy}+\delta^2\theta_{xx}\right)+N_{TC}\left(\delta^2\gamma_{xx}+\gamma_{yy}\right)\\ &\quad + N_b\left(\delta^2\Omega_x\theta_x+\theta_y\Omega_y\right),\end{aligned} \tag{14}$$

$$\mathrm{Re}\delta Le\left(\Psi_y\gamma_x-\Psi_x\gamma_y\right) = \left(\delta^2\gamma_{xx}+\gamma_{yy}\right)+N_{CT}\left(\delta^2\theta_{xx}+\theta_{yy}\right), \tag{15}$$

$$\begin{aligned}\mathrm{Re}\delta Ln\left(\Psi_y\Omega_x-\Psi_x\Omega_y\right) &= \left(\delta^2\Omega_{xx}+\Omega_{yy}\right)\\ &\quad + \frac{N_t}{N_b}\left(\delta^2\theta_{xx}+\theta_{yy}\right).\end{aligned} \tag{16}$$

Now, imposing constraints of Re − > 0 (low Reynolds number) and $\delta \ll 1$ (long wavelength), the equations. (19)-(23) are now reduced as follows:

$$\begin{aligned}0 &= -\frac{\partial p}{\partial x}+\frac{\partial S_{xy}}{\partial y}-M^2\cos^2\beta\left(\Psi_y+1\right)\\ &\quad + G_{rt}\theta+G_{rc}\gamma-G_{rF}\Omega,\end{aligned} \tag{17}$$

$$0 = -\frac{\partial p}{\partial y}, \tag{18}$$

$$\frac{\partial^2\theta}{\partial y^2}+N_{TC}\frac{\partial^2\gamma}{\partial y^2}+N_b\left(\frac{\partial\theta}{\partial y}\frac{\partial\Omega}{\partial y}\right)+N_t\left(\frac{\partial\theta}{\partial y}\right)^2 = 0, \tag{19}$$

$$\frac{\partial^2\gamma}{\partial y^2}+N_{CT}\frac{\partial^2\theta}{\partial y^2} = 0, \tag{20}$$

$$\frac{\partial^2\Omega}{\partial y^2}+\frac{N_t}{N_b}\frac{\partial^2\theta}{\partial y^2} = 0, \tag{21}$$

Now, taking pressure out of (17) and (18) yields the following expression as follows:

$$\frac{\partial^2 S_{xy}}{\partial y^2}-M^2\cos^2\beta\frac{\partial^2\Psi}{\partial y^2}+G_{rt}\frac{\partial\theta}{\partial y}+G_{rc}\frac{\partial\gamma}{\partial y}-G_{rF}\frac{\partial\Omega}{\partial y} = 0, \tag{22}$$

where the dimensionless equation for S_{xy} is obtained from equation (7)and expressed as follows:

$$S_{xy} = \left[\frac{1+2\eta_1\left(\partial^2\Psi/\partial y^2\right)^2}{1+2\eta_2\left(\partial^2\Psi/\partial y^2\right)^2}\right]\left(\frac{\partial^2\Psi}{\partial y^2}\right), \tag{23}$$

in which $\eta_1 = \lambda_2\lambda_3$ and $\eta_2 = \lambda_1\lambda_3$. Now, if $\eta_1 = \eta_2$ the model of Oldroyd-4 constant fluid reduces to viscous fluid.

The expression for Q (mean flow) is computed in the dimensionless form as follows:

$$Q = F + 1 + d, \tag{24}$$

where

$$\begin{aligned}F &= \int_{h_2(x)}^{h_1(x)}\frac{\partial\Psi}{\partial y}\mathrm{d}y = \Psi\left(h_1(x)-h_2(x)\right),\\ h_1(x) &= 1+a\cos 2\pi x,\\ h_2(x) &= -d-b\cos\left(2\pi x+\varphi\right).\end{aligned} \tag{25}$$

For the problem under investigation, the slip boundary conditions in dimensionless forms are defined as follows:

$$\begin{aligned}&\Psi = \frac{F}{2}, \frac{\partial\Psi}{\partial y}+\varepsilon_1 S_{xy} = -1 \text{ on } y = h_1(x),\\ &\Psi = -\frac{F}{2}, \frac{\partial\Psi}{\partial y}-\varepsilon_1 S_{xy} = -1 \text{ on } y = h_2(x),\\ &\theta+\varepsilon_2\frac{\partial\theta}{\partial y} = 0, \text{ on } y = h_1,\\ &\theta-\varepsilon_2\frac{\partial\theta}{\partial y} = 1, \text{ on } y = h_2,\\ &\gamma+\varepsilon_3\frac{\partial\gamma}{\partial y} = 0, \text{on } y = h_1,\\ &\gamma-\varepsilon_3\frac{\partial\gamma}{\partial y} = 1, \text{ on } y = h_2,\\ &\Omega+\varepsilon_4\frac{\partial\Omega}{\partial y} = 0, \text{ on } y = h_1,\\ &\Omega-\varepsilon_4\frac{\partial\Omega}{\partial y} = 1, \text{ on } y = h_2.\end{aligned} \tag{26}$$

If $\varepsilon_1, \varepsilon_2\varepsilon_3\varepsilon_4 = 0$ in the parameters, then no slip conditions exist.

3.1. Special Cases

3.1. Special Cases. In the absence of slip conditions ($\varepsilon_1 = \varepsilon_2 = \varepsilon_3 = \varepsilon_4 = 0$), $M = 0, G_{rt} = 0$, $G_{rc} = 0, G_{rF} = 0$, and $\eta_1 = \eta_2$ the findings of reference [4] can also be recovered as a limited case of existing problem.

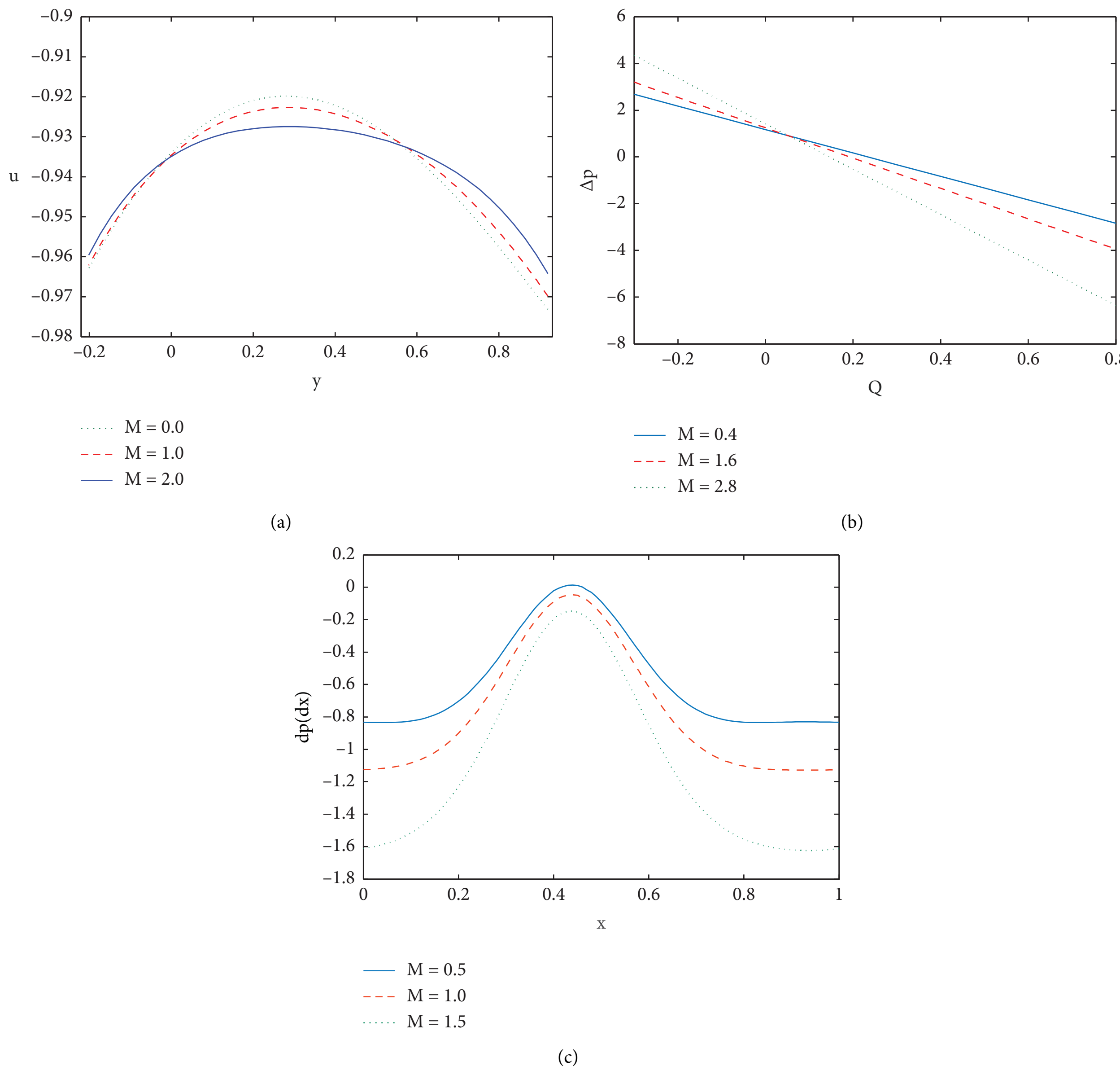

Figure 2: Influence of the Hartmann number (M) on $u\Delta p$ and dp/dx.

4. Numerical Solution and Graphical Outcomes

Numerical simulations become essential as analytical solutions can only be found for a limited number of cases. Numerical simulations provide us an alternative mean to understand the problem and its solution without wasting the real resources that are involved in the study. We can develop a comprehensive understanding of the flow situations using modern tools available in the form of software's like: MATLAB, MATHEMATICA, and ANSYS. The main objective of the present work is to evaluate the consequence of double-diffusion convection and partial slip on magneto-Oldroyd-4 constants nanofluids with peristaltic propulsion in an asymmetric channel. The exact solutions of the equations (24)-(29) are not easy to evaluate due to coupled and highly nonlinear characteristics. Therefore, the regressive equations are numerically solved in MATHEMATICA by using built-in command ND-Solve. Solutions are utilized in obtaining pressure gradient, pressure rise, and streamlines for different flow parameters. The graphical results are also established employing numerical solutions to verify that numerical data are accurate and to examine the impact of a variety of flow parameters.

4.1. Effects of the Hartmann Number. The Hartmann number is described as ratio of electromagnetic force to viscous force. It is a regular occurrence in fluid flows passing via magnetic fields. Figures 2(a) to 2(c) explain the impact of velocity profile, pressure rise, and pressure gradient on the Hartmann number M. As Hartmann number enhances, the magnitude of the velocity profile

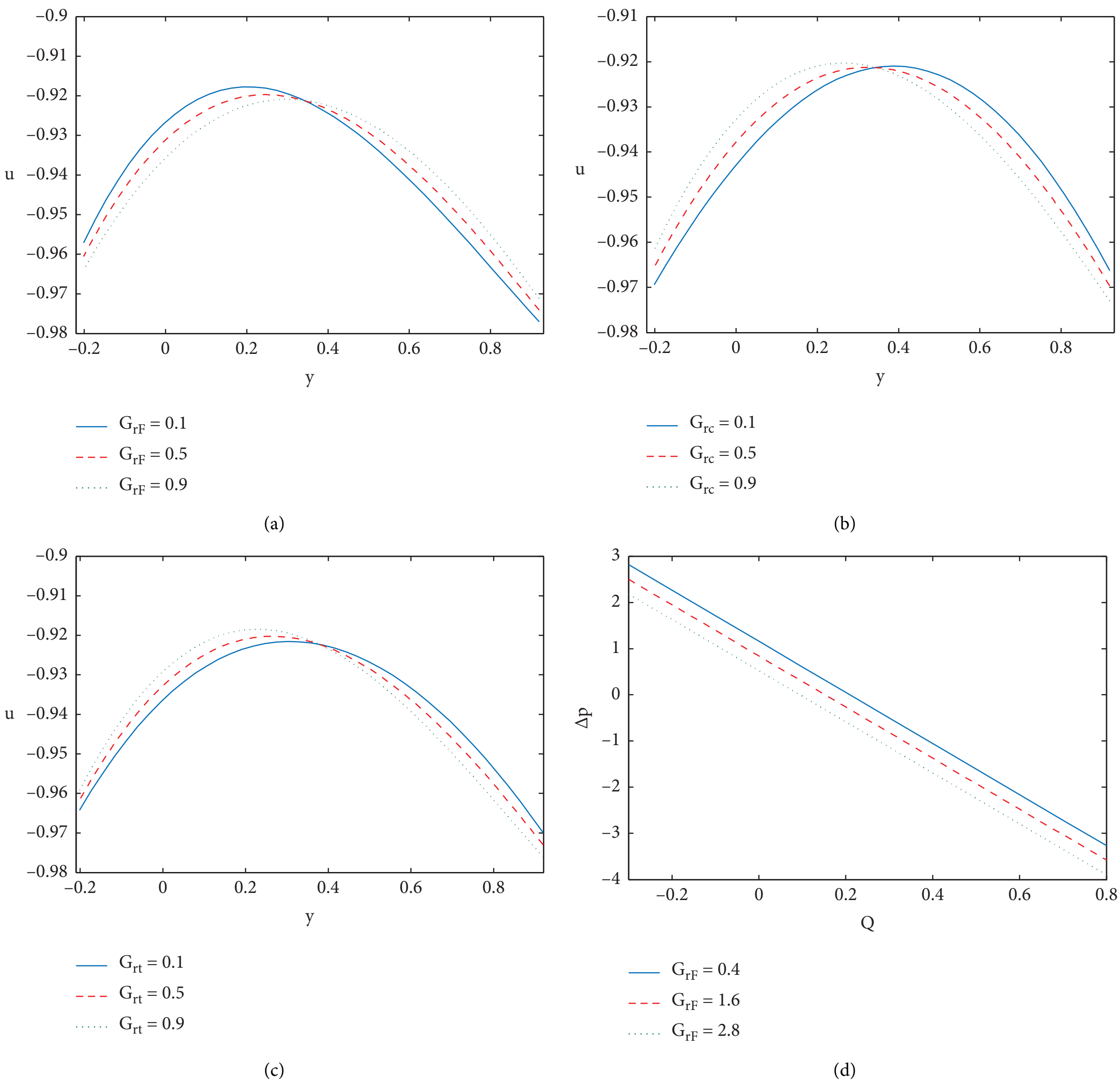

FIGURE 3: Continued.

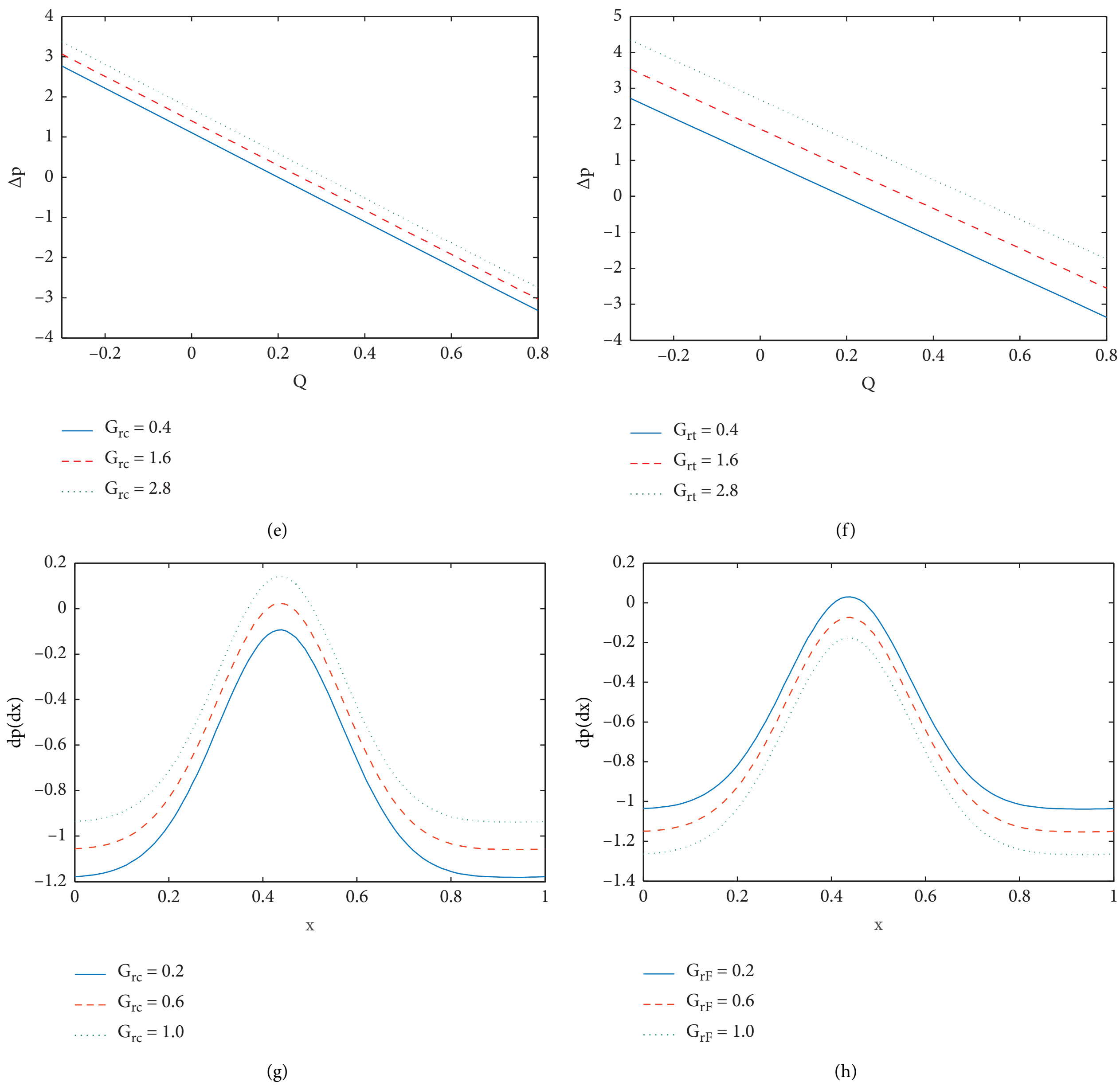

FIGURE 3: Influence of nanoparticle (G_{rF}), solutal (G_{rc}), and thermal (G_{rt}) Grashof numbers on u, Δp, and dp/dx.

significantly reduces in channel's center and tends to increase near peristaltic walls (see Figure 2(a)). Furthermore, the profile of velocity has a parabolic shape. In fact, enhancing magnetic number causes the Lorentz force to increase, which tends as a retarding force and slowing fluid motion. Figure 2(b) depicts M'sresponse to pressure rise. It is illustrated in Figure 2(b) that increasing M causes pressure rise to increase in peristaltic $(Q>0, \Delta p>0)$, retrograde $(Q<0, \Delta p>0)$, and free $(\Delta p=0)$ pumping zones. Moreover, it reduces in the augmented $(Q>0, \Delta p<0)$ pumping zone due to higher values of M. The pressure gradient continues to decrease as the Hartmann number rises (see Figure 2(c)).

4.2. Effects of Nanoparticle (G_{rF})*, Solutal* (G_{rc})*, and Thermal* (G_{rt}) *Grashof Numbers.* In fluid dynamics and heat transfer, the Grashof numbers are described by ratio of buoyancy to viscous force that acts on a fluid. The consequence of nanoparticle, solutal, and thermal Grashof numbers on velocity profile is illustrated in Figures 3(a) to 3(c). The magnitudes of the flow velocity rises when $y \in [-0.2, 0.35]$ by enhancing G_{rF}, while opposite phenomenon occurs when $y \in [0.35, 0.87]$. Here magnitude of velocity field drops (see Fig. 3(a)). This happens because nanoparticles viscosity drops, causing the velocity to decrease. In Figure 3(b) and 3(c), it is noted that magnitudes of fluid velocity drops when $y \in [-0.2, 0.35]$ but it increases when

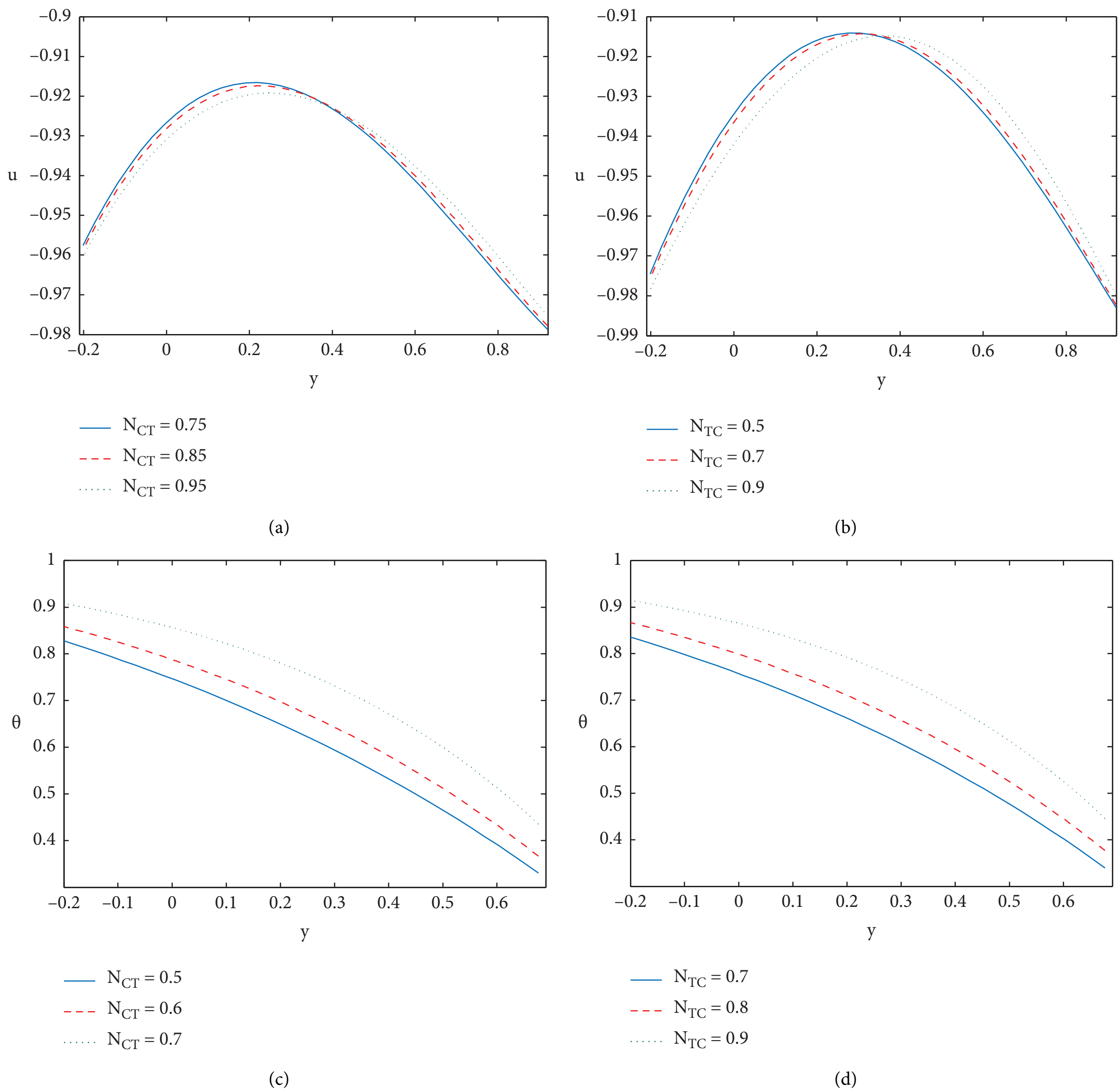

Figure 4: Continued.

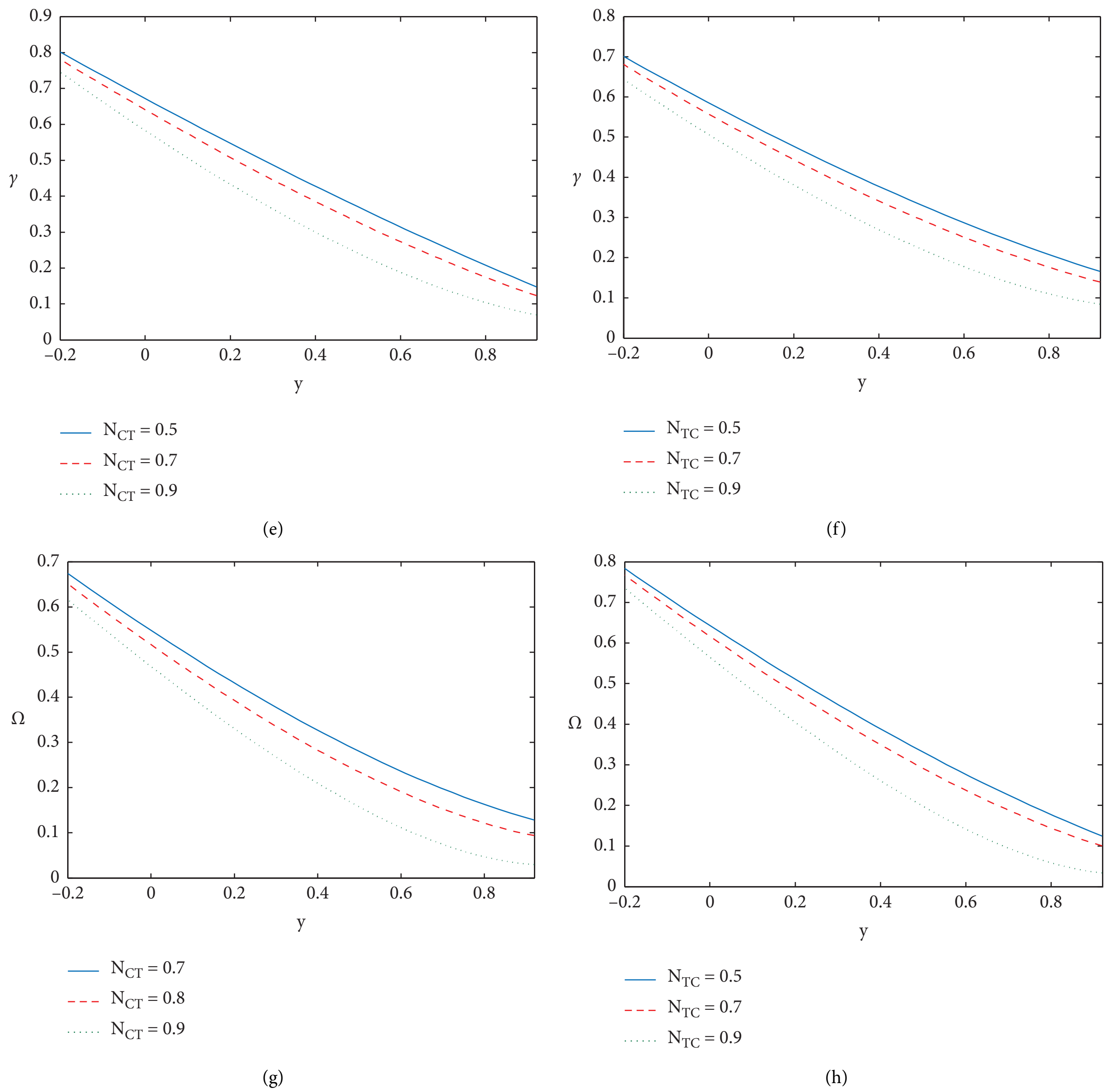

FIGURE 4: Effects of Soret (N_{CT}) and Dufour (N_{TC}) parameters on u, θ, γ, and Ω.

$y \in [0.35, 0.87]$ by enhancing G_{rc} and G_{rt}. In most instances, thermal buoyancy serves to slow down the flow in the regime. The behavior of pressure rise for G_{rF}, G_{rc}, and G_{rt} is demonstrated in Figures 3(d) to 3(f). It is noted in Figure 3(d) that in all peristaltic regions (augmented $(Q > 0, \Delta p < 0)$, free ($\Delta p = 0$), augmented $(Q > 0, \Delta p < 0)$, and retrograde $(Q < 0, \Delta p > 0)$) the pressure rise drops by rising G_{rF} values. On the other hand, G_{rc} and G_{rt} exhibit the opposite trend. Here, pressure rises in all peristaltic zones are increased by boosting G_{rc} and G_{rt} values (see Figure 3(e) and 3(f)). The roll of pressure gradient for G_{rc} and G_{rF} are explained in Figure 3(g) and 3(h). It is indicated in Figure 3(g) that the pressure gradient significantly increases when values of G_{rc} increases. The pressure gradient tends to reduce when G_{rF} increases (see Figure 3(h)).

4.3. Effects of Soret (N_{CT}) *and Dufour* (N_{TC}) *Parameters.* The outcomes of Soret and Dufour constraints are shown in Figures 4(a) to 4(h). It is shown in Figures 4(a) and 4(b) that N_{CT} and N_{TC} have a similar behavior on the velocity profile, as already explained in Figure 3(a). Figures 4(c) and 4(d) depict the impact of N_{CT} and N_{TC} on temperature profile. The temperature increases by increasing N_{CT} and N_{TC}. It is only because temperature has a direct connection with the constraints of Soret and Dufour. The concentration and

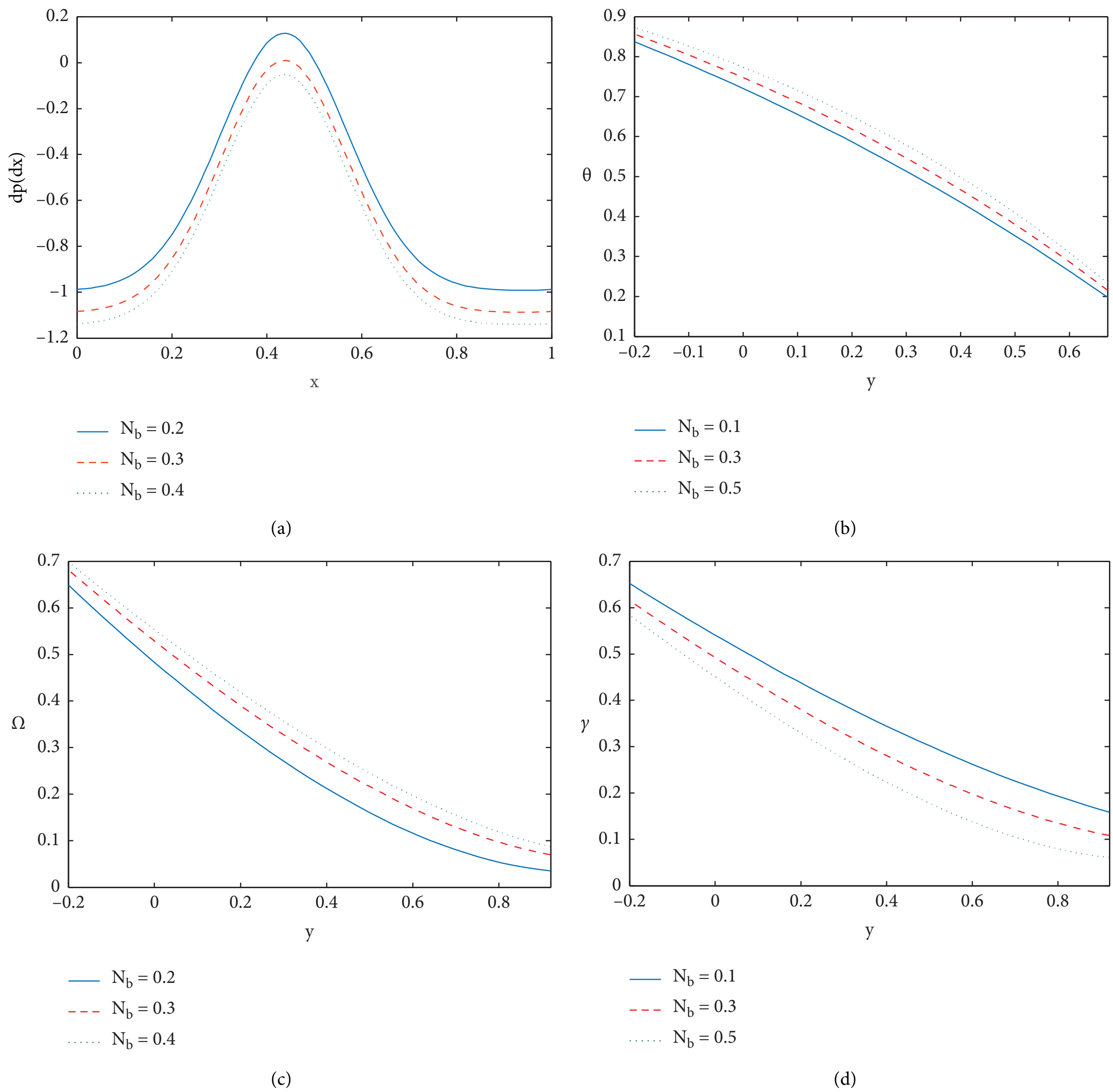

FIGURE 5: Effects of N_b on dp/dx, θ, Ω, and γ.

nanoparticle fraction profiles decrease by enhancing N_{CT} and N_{TC} values (see Figures 4(e) to 4(h)). Its because random motion reacts with micromixing and random collision tendency of solid nanoparticle, spreading the solid nanoparticles and lessening solute concentration.

4.4. Effects of the Brownian Motion (N_b) Parameter. Figures 5(a) to 5(d) look at the impact of the Brownian motion on $dp/dx\theta\gamma$ and Ω. It is clear from Figure 5(a) that by increasing N_b values pressure gradient drops. The temperature and nanoparticle fraction increase by increasing N_b values (see Figures 5(b) and 5(c)). When the Brownian motion gets more vigorous, the nanoparticles are effectively transferred from wall to fluid. The temperature rises as N_b rises as an outcome of this interaction. Furthermore, nanoparticle volume fraction has a direct relationship with N_b. The adverse trends are noted for the case of concentration. Here, by rising N_b values, the concentration drops (see Figure 5(d)). In nature, the nanofluid is just a two-phase fluid, and stochastic mobility of isolated nanoparticles increases energy exchange rates while dropping concentrations in the fluid flow.

4.5. Effects of the Thermophoresis (N_t) Parameter. The roll of velocity, concentration, temperature, nanoparticle fraction, and pressure gradient on N_t are indicated in Figures 6(a)–

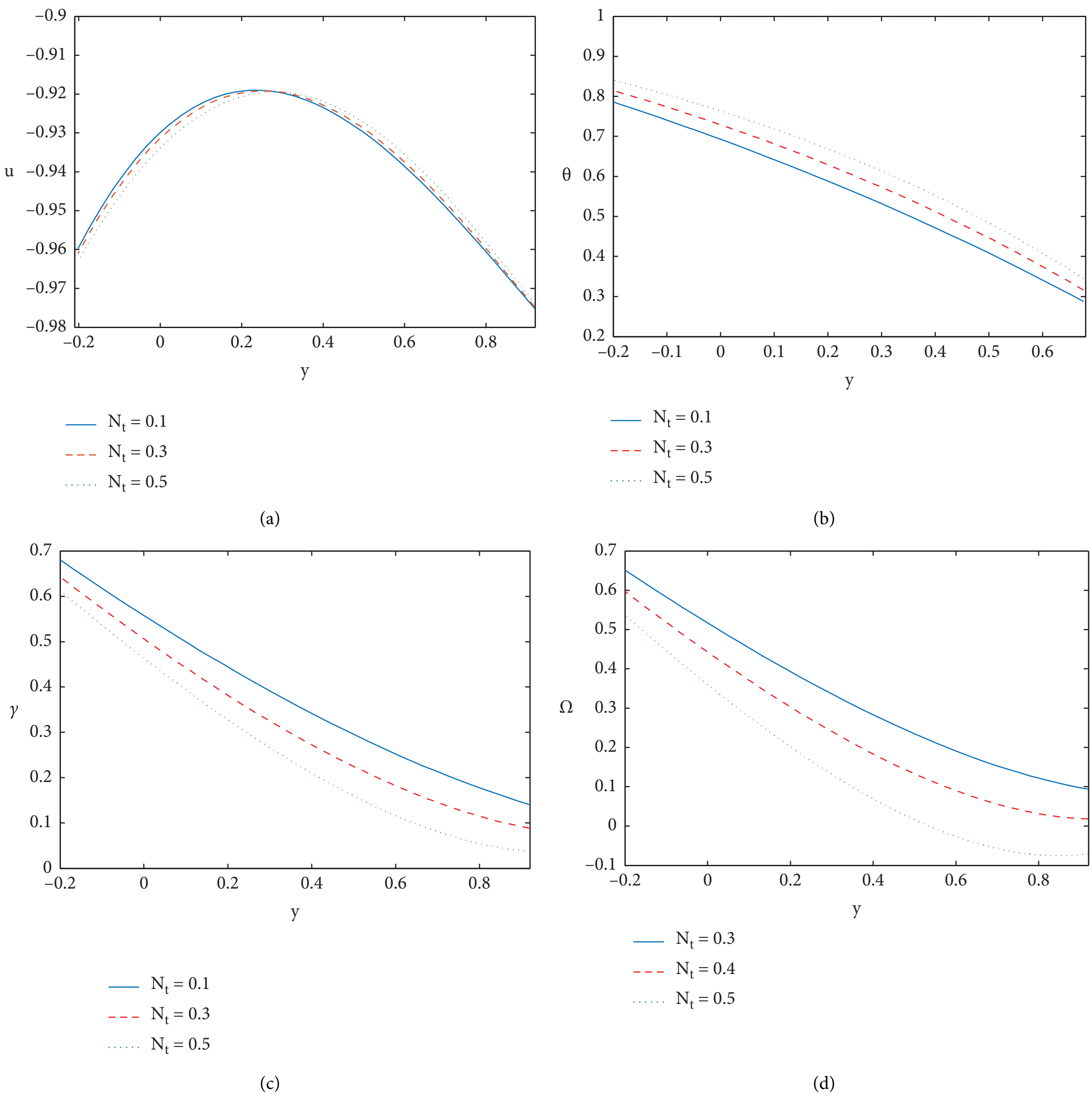

Figure 6: Continued.

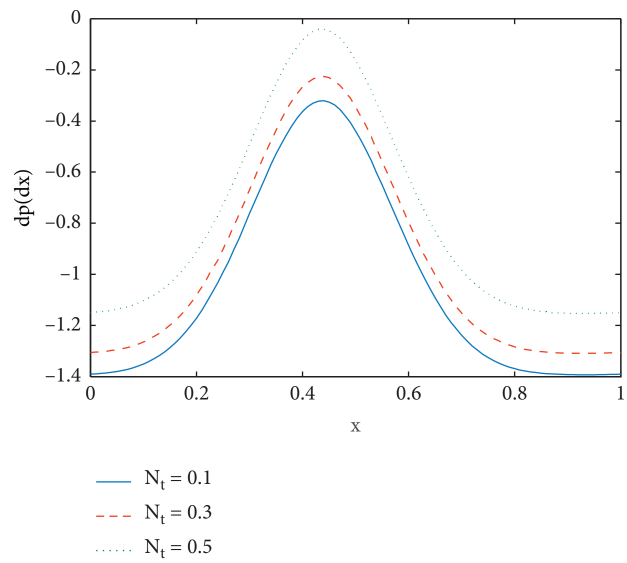

(e)

Figure 6: Effects of N_t on u, θ, γ, Ω, and dp/dx.

6(e). The outcomes of altering the thermophoresis coefficient on the flow velocity are seen in Figure 6(a). When value of thermophoresis parameters rises the magnitude of flow velocity, it increases in the zone $y \in [-0.2, 0.3]$. Furthermore, it tends to fall when $y \in [0.3, 0.86]$. The velocity of fluid is maximum near the channel's center. The role of N_t on temperature is shown in Figure 6(b). It shows that N_b and N_t have an identical behavior of fluid temperature, as already shown in Figure 5(b). The slightly different effects are noted for the case of concentration and nanoparticle fraction (see Figures 6(c) and 6(d)). Here, due to the rising tendency of N_t, the concentration and nanoparticle fraction decreases. The occurrence of pressure gradient is elaborated in Figure 6(e). It is noted in Figure 6(e) that pressure gradient falls as thermophoresis parameter rises.

4.6. Effects of Slip Parameters ($\varepsilon_1 - \varepsilon_4$). The outcomes of parameters of slip-on velocity, concentration, temperature, nanoparticle fraction pressure gradient, and pressure rise are shown in Figures 7(a) to 7(g). It is noted in Figure 7(a) that nature of velocity curve is parabolic. Moreover, by increasing parameter of velocity slip, the magnitude of flow velocity tends to fall when $y \in [-0.2, 0.1]$ and $y \in [0.65, 0.86]$ but reverse effects are noted when $y \in [0.1, 0.65]$, here magnitude of flow velocity increases. The impact of temperature slip ε_2 is shown in Figure 7(b). It is indicated in Figure 7(b) that by enhancing temperature slip ε_2 temperature drops in the region $y \in [-0.2, -0.1]$ but it tends to rise in region $y \in [-0.1, 0.65]$. The kinetic energy of particles of fluid increases due to slip which rises the fluid temperature. Figures 7(c) and 7(d) depict the influence of parameters of slip concentration ε_3 and slip nanoparticle fraction ε_4. There is a fall in concentration and nanoparticle fraction in the region $y \in [-0.2, 0.65]$ due to the rising values of slip parameter of concentration and slip factor of nanoparticle fraction. Furthermore, opposite effects are noted in the region $y \in [0.65, 0.85]$ (see Figure 7(c) and 7(d)). The particle of fluid is interrupted less by the walls of channel, so concentration drops as the value of ε_3 increases. Hence, the rate of mass transfer of nanoparticles is slowed. The role of pressure rise on velocity slip ε_1 is drawn in Figure 7(e). It is indicated in Figure 7(e) that pressure rise reduces in augmented and retrograde pumping zones but increases in augmented region by increasing velocity slip constraints. The pressure gradient increases due to the increasing behaviour of velocity slip constraints ε_1 and nanoparticle slip factor ε_4 (see Figures 7(f) and 7(g)).

4.7. Effects of Non-Newtonian Parameters (η_1 and η_2). To discuss the roll of non-Newtonian parameters η_1 and η_2 on pressure rise, pressure gradient, and velocity, Figures 8(a) to 8(e) are displayed. It is exhibited in Figures 8(a) and 8(b) that η_1 and η_2 shows similar behavior on pressure rise. It is illustrated in Figures 8(a) and 8(b) that by increasing η_1 and η_2, pressure rise increases in peristaltic and free and retrograde pumping areas but reduces in the augmented region. The pressure gradient is maximum at channel's center, but near the channel wall's pressure gradient drops due to the increasing values of non-Newtonian parameters η_1 and η_2 (see (Figures 8(c) and 8(d)). It is shown in Figure 8(e) that M and (η_1, η_2) have an identical behavior on fluid velocity, as already explain in Figure 2(a).

4.8. Trapping Phenomenon. Trapping is an unusual occurrence in peristaltic propelling flows. It is begun by the development of a fluid mass that internally moves and is enclosed by streamlines of peristaltic wave. Streamlines capture the mass bolus of fluid and move it forward using waves of peristaltic at high flow rates and significant

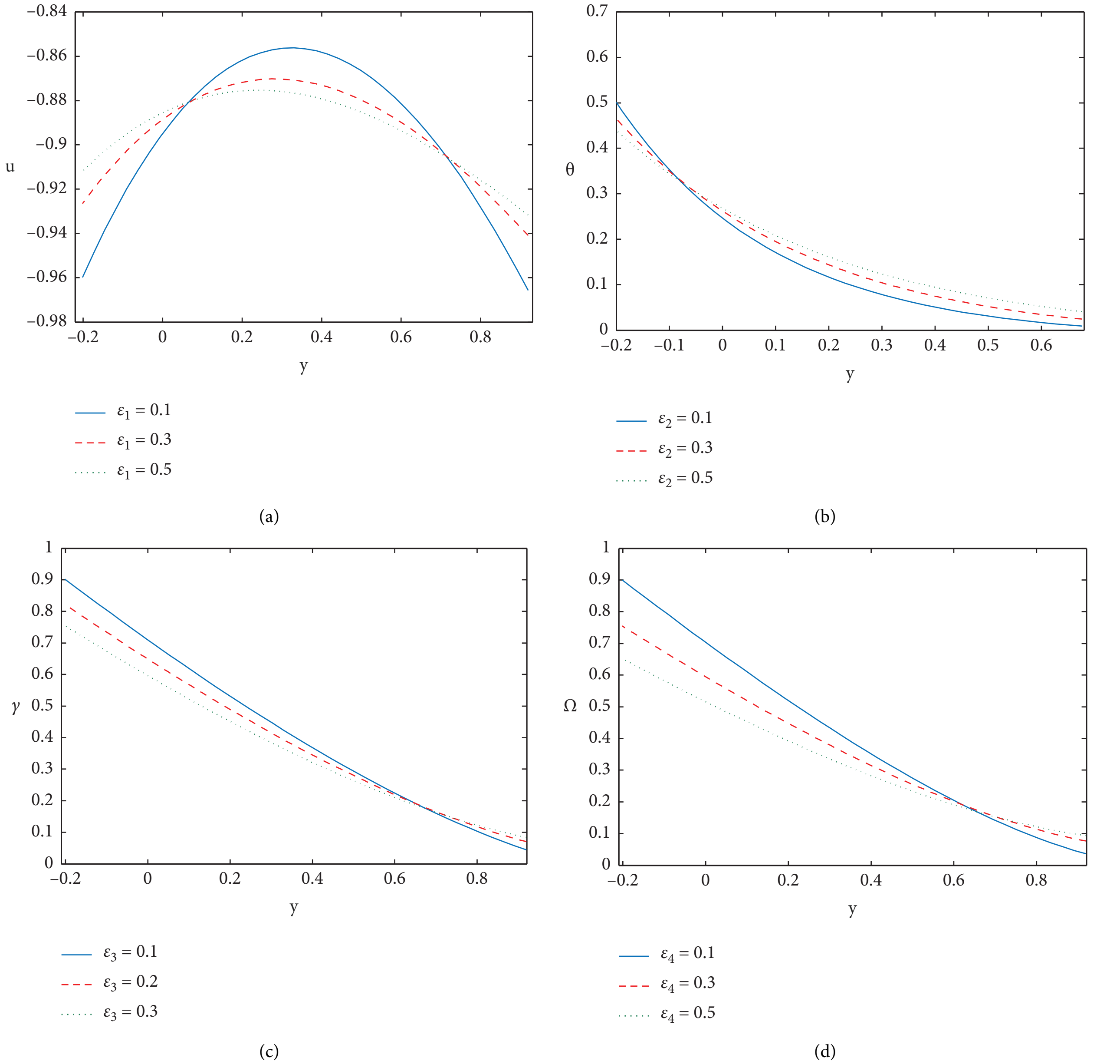

Figure 7: Continued.

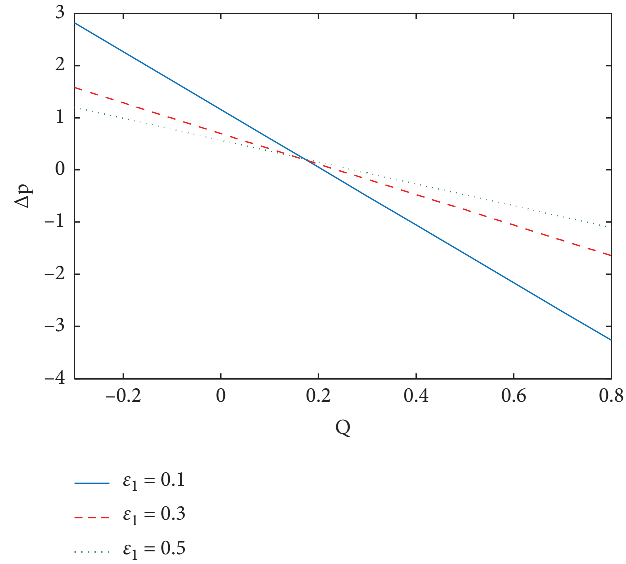

(e)

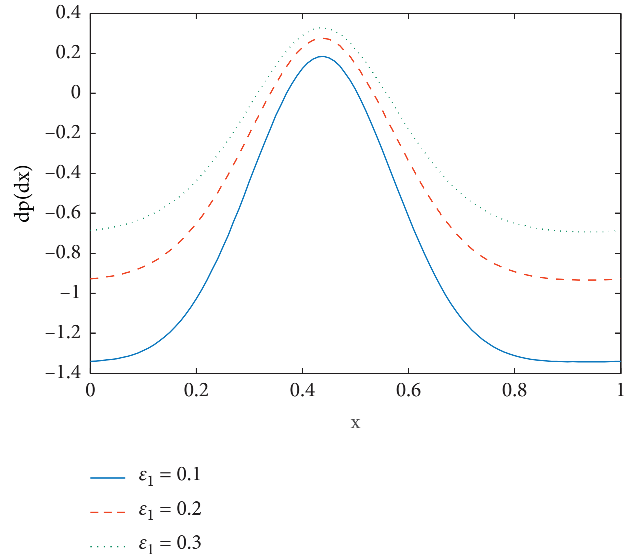

(f)

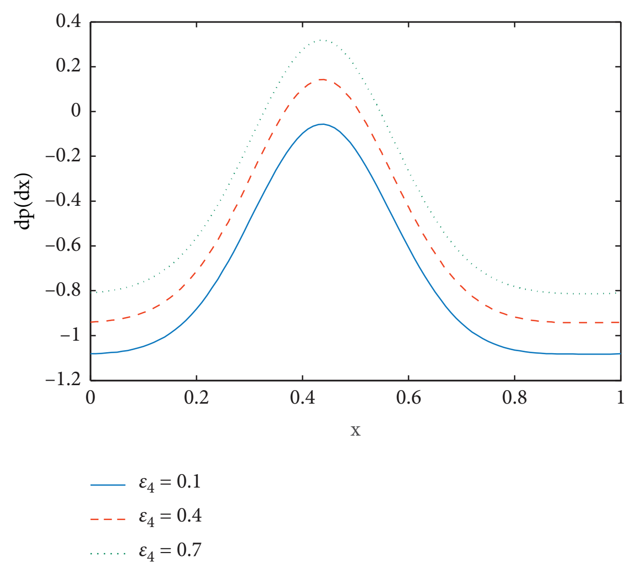

(g)

Figure 7: Effects of slip parameters on u, θ, γ, Ω, Δp, and dp/dx.

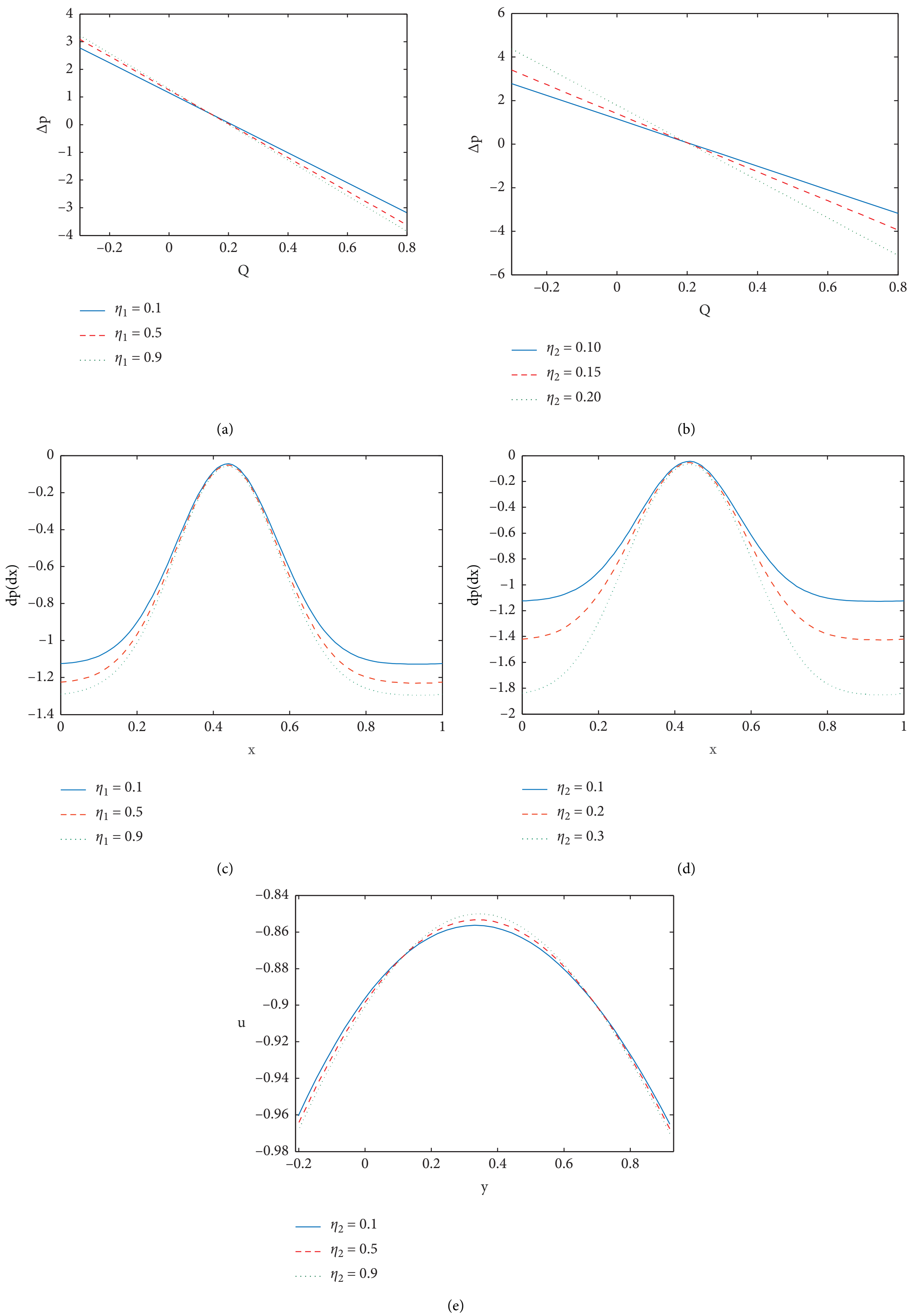

Figure 8: Effects of non-Newtonian parameters (η_1,η_2) on Δp,dp/dx, and u.

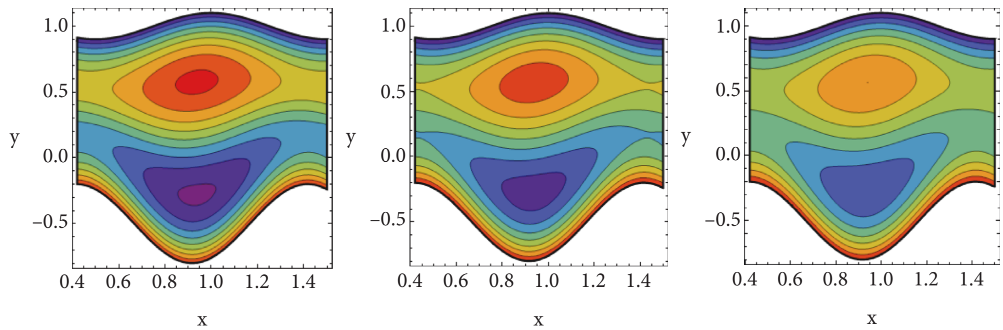

$\omega_1 = 0.10$ $\omega_1 = 0.15$ $\omega_1 = 0.20$

FIGURE 9: Impact of streamlines on ω_1.

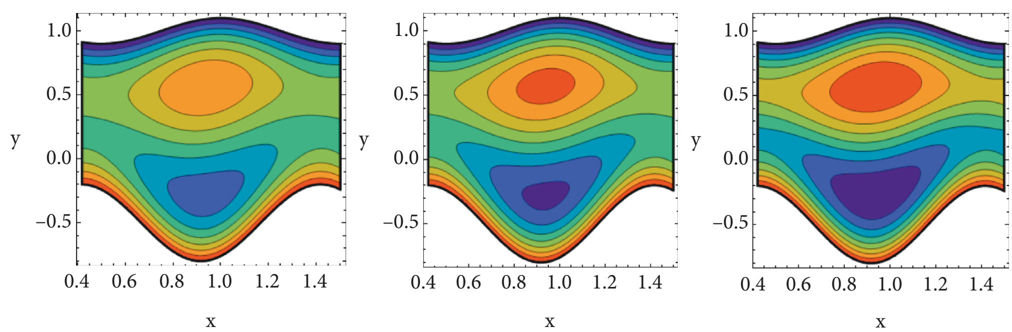

$\eta_2 = 0.01$ $\eta_2 = 0.05$ $\eta_2 = 0.09$

FIGURE 10: Impact of streamlines on η_2.

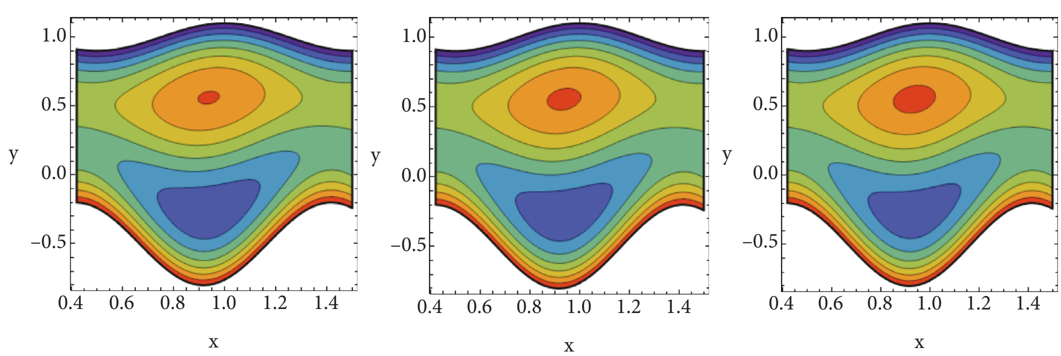

$G_{rt} = 0.5$ $G_{rt} = 1.0$ $G_{rt} = 1.5$

FIGURE 11: Impact of streamlines on G_{rt}.

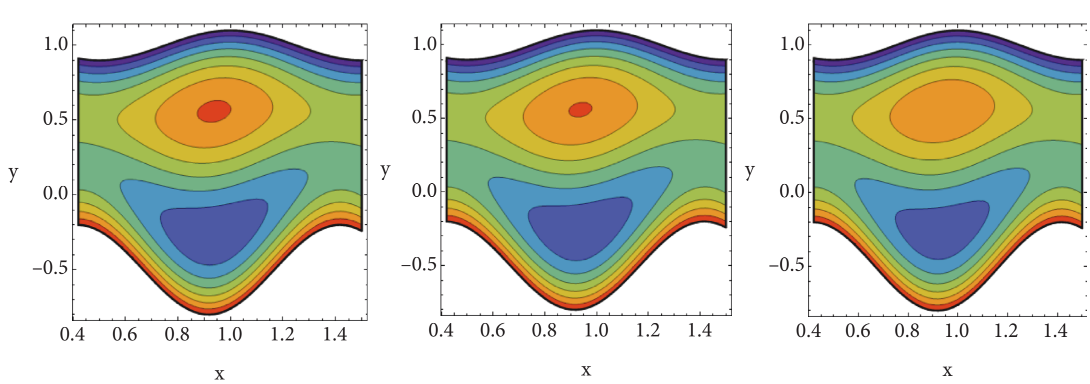

$M = 0.0$ $M = 1.0$ $M = 2.0$

FIGURE 12: Impact of streamlines on M.

Table 1: A comparison with the existing literature.

$y = h(x)$	Velocity profile $u(x)$	
	Present work (with partial slip)	Viscous fluid [4](without partial slip)
0.919093	−0.973134	−1
0.80702	−0.958414	−0.960643
0.694947	−0.945033	−0.932377
0.582873	−0.933854	−0.914322
0.4708	−0.925582	−0.9056
0.358727	−0.920802	−0.90533
0.246653	−0.919989	−0.912633
0.13458	−0.923532	−0.926632
0.0225065	−0.931737	−0.946445
−0.0895668	−0.944838	−0.971194
−0.20164	−0.963001	−1

occlusions. It is indicated in Figure 9 that due to the increasing behavior of velocity slip factor ε_1 size of trapped bolus increases and amount of trapped bolus reduces in both upper and lower portion of channel. By increasing non-Newtonian parameters, η_2 streamlines show that the trapped bolus size enhances (see Figure 10). In Figure 11, it is illustrated that the trapped bolus volume grows as the thermal Grashof number G_{rt} rises. The reverse behavior is noted for the Hartmann number M case. Here, the size reduces by rising values of M (see Figure 12).

Table 1 shows the comparison with the existing literature.

5. Conclusion

The main objectives of this paper are to examine the effect of double-diffusion convection and partial slip with a tilted magnetic field on peristaltic movement in an asymmetric channel for the Oldroyd-4 constants nanofluids. A numerical methodology is used to solve nonlinear system of PDEs. The impact of several physiological parameters on flow quantities is visually depicted. Based on our analysis, it was found that the nanoparticle fraction and concentration profile decrease by boosting slip factors of concentration and nanoparticles. Also, the velocity profiles can be controlled by adjusting the parameters under observation (like slip parameter, non-Newtonian parameter, and diffusivity parameters). Throughout the velocity profiles, it is observed that velocity tend to increase, reach its maximum value, and then decreases to meet the boundary condition while moving from one end to the other. It was also found that the profile of temperature rises as the Brownian motion and thermophoresis constraints increases. This is because growth in the Brownian motion parameter indicates the increase in the kinetic energy of nanoparticles which results in warming up the nanofluid. Physically, thermophoresis demonstrates the temperature difference of nanofluid in the channel walls, and as a result, the temperature rises as the values of the associated parameters are increased. Also, concentration drops as the Brownian motion and thermophoresis constraints increases. Another main finding of the study is that shape of trapped bolus decreases as the Hartmann number increases. This means that by making electromagnetic forces dominant as compared to viscous forces can be effective in drug delivery. Lastly, the confined bolus size grows as the thermal Grashof number rises since buoyancy force becomes dominant as compared to viscous forces.

Nomenclature

C: Solutal concentration
M: Hartmann number
T: Temperature
Pr: Prandtl number
G_{rF}: Grashof number of nanoparticles
Le: Lewis number
Ω: Nanoparticle volume fraction
N_b: Brownian motion parameter
D_B: Brownian diffusion coefficient
D_T: Thermophoretic diffusion coefficient
Re: Reynolds number
G_{rt}: Thermal Grashof number
D_s: Solutal diffusively
N_{TC}: Dufour parameter
N_t: Thermophoresis parameter
Ln: Nanofluid Lewis number
$(\rho c)_f$: Heat capacity of fluid
$(\rho c)_p$: Heat capacity of nanoparticle
N_{CT}: Soret parameter
D_{TC}: Dufour diffusively
G_{rc}: Solutal Grashof number
D_{CT}: Soret diffusively

Small alphabets

u: Axial velocity
v: Transverse velocity
g: Acceleration due to gravity
b: Wave amplitude
d_1, d_3: Channel width
p: Pressure
k: Thermal conductivity
t: Time
d_2, d_4: Wave amplitudes
c: Propagation of velocity

Greek symbols

δ: Wavelength
Ψ: Stream function
ρ_p: Nanoparticle mass density
$(\rho c)_p$: Nanoparticle heat capacity
γ: Solutal concentration
ω: Magnetic field inclination angle
β_T: Volumetric coefficient of thermal expansion
β_C: Volumetric coefficient of solutal expansion
ε_3: Concentration slip parameter
ε_4: Nanoparticles slip parameter
ε_1: Velocity slip parameter
ε_2: Temperature slip parameter
δ: Wave number
Θ: Temperature
ρ_f: Fluid density
ρ_{f_0}: Fluid density at T_0.

Data Availability

No data were used to support this study.

Conflicts of Interest

All authors declare that there are no conflicts of interest for this manuscript.

Acknowledgments

The authors extend their appreciation to the Deanship of Scientific Research, University of Hafr Al Batin, for funding this work through the research group project no. (0033-1443-S).

References

[1] T. W. Latham, *Fluid Motion in a Peristaltic Pump*, MIT, Cambridge, 1966.
[2] A. H. Shapiro, M. Y. Jaffrin, and S. L. Weinberg, "Peristaltic pumping with long wavelengths at low Reynolds number," *Journal of fluid mechanics*, Cambridge University Press, vol. 37, pp. 799–825, 1969.
[3] N. Ijaz, A. Riaz, A. Zeeshan, R. Ellahi, and S. M. Sait, "Buoyancy driven flow with gas-liquid coatings of peristaltic bubbly flow in elastic walls," *Coatings*, vol. 10, no. 2, p. 115, 2020.
[4] M. Mishra and A. Ramachandra Rao, "Peristaltic transport of a Newtonian fluid in an asymmetric channel," *Zeitschrift fur Angewandte Mathematik und Physik (ZAMP)*, vol. 54, no. 3, pp. 532–550, 2003.
[5] M. V. S. Reddy, M. Mishra, S. Sreenadh, and A. R. Rao, "Influence of lateral walls on peristaltic flow in a rectangular duct," *Journal of Fluids Engineering*, vol. 127, no. 4, pp. 824–827, 2005.
[6] A. E. H. Abd El Naby and A. E. M. El Misiery, "Effects of an endoscope and generalized Newtonian fluid on peristaltic motion," *Applied Mathematics and Computation*, vol. 128, no. 1, pp. 19–35, 2002.
[7] R. Ellahi, A. Riaz, S. Nadeem, and M. Ali, "Peristaltic flow of Carreau fluid in a rectangular duct through a porous medium," *Mathematical Problems in Engineering*, vol. 2012, Article ID 329639, 24 pages, 2012.
[8] T. Hayat, N. Ali, and S. Asghar, "Hall effects on peristaltic flow of a Maxwell fluid in a porous medium," *Physics Letters A*, vol. 363, no. 5-6, pp. 397–403, 2007.
[9] Y. Wang, T. Hayat, and K. Hutter, "Peristaltic flow of a Johnson Segalman fluid through a deformable tube," *Theoretical and Computational Fluid Dynamics*, vol. 21, no. 5, pp. 369–380, 2007.
[10] S. Nadeem and S. Akram, "Peristaltic flow of a Williamson fluid in an asymmetric channel," *Communications in Nonlinear Science and Numerical Simulation*, vol. 15, no. 7, pp. 1705–1716, 2010.
[11] J. Venkatesan, D. S. Sankar, K. Hemalatha, and Y. Yatim, "Mathematical analysis of Casson fluid model for blood rheology in stenosed narrow arteries," *Journal of Applied Mathematics*, vol. 2013, Article ID 583809, 2013.
[12] S. N. Aristov and O. I. Skul'skii, "Exact solution of the problem on a six-constant Jeffreys model of fluid in a plane channel," *Journal of Applied Mechanics and Technical Physics*, vol. 43, no. 6, pp. 817–822, 2002.
[13] S. Nadeem and N. S. Akbar, "Peristaltic flow of Walter's B fluid in a uniform inclined tube," *Journal of Biorheology*, vol. 24, no. 1, pp. 22–28, 2010.
[14] S. Nadeem and S. Akram, "Peristaltic transport of a hyperbolic tangent fluid model in an asymmetric channel," *Zeitschrift für Naturforschung A*, vol. 64, no. 9-10, pp. 559–567, 2009.
[15] K. Vajravelu, S. Sreenadh, P. Devaki, and K. V. Prasad, "Mathematical model for a Herschel-Bulkley fluid flow in an elastic tube," *Open Physics*, vol. 9, no. 5, pp. 1357–1365, 2011.
[16] A. M. Abd Alla and S. M. Abo Dahab, "Magnetic field and rotation effects on peristaltic transport of a Jeffrey fluid in an asymmetric channel," *Journal of Magnetism and Magnetic Materials*, vol. 374, pp. 680–689, 2015.
[17] N. T. M. El Dabe, A. Y. Ghaly, S. N. Sallam, K. Elagamy, and Y. M. Younis, "Peristaltic pumping of a conducting Sisko fluid through porous medium with heat and mass transfer," *American Journal of Computational Mathematics*, vol. 05, no. 03, pp. 304–316, 2015.
[18] N. Ali, Y. Wang, T. Hayat, and M. Oberlack, "Long wavelength approximation to peristaltic motion of an Oldroyd 4-constant fluid in a planar channel," *Biorheology*, vol. 45, no. 5, pp. 611–628, 2008.
[19] K. Vajravelu, S. Sreenadh, P. Lakshminarayana, G. Sucharitha, and M. M. Rashidi, "Peristaltic flow of phan-thien-tanner fluid in an asymmetric channel with porous medium," *Journal of Applied Fluid Mechanics*, vol. 9, no. 6, pp. 1615–1625, 2016.
[20] D. Tripathi, S. K. Pandey, and S. Das, "Peristaltic transport of a generalized Burgers' fluid: application to the movement of chyme in small intestine," *Acta Astronautica*, vol. 69, no. 1-2, pp. 30–38, 2011.
[21] J. C. Misra and S. D. Adhikary, "Flow of a Bingham fluid in a porous bed under the action of a magnetic field: application to magneto-hemorheology," *Engineering Science and Technology, an International Journal*, vol. 20, no. 3, pp. 973–981, 2017.
[22] S. Haider, N. Ijaz, A. Zeeshan, and Y. Z. Li, "Magneto-hydrodynamics of a solid-liquid two-phase fluid in rotating channel due to peristaltic wavy movement," *International Journal of Numerical Methods for Heat and Fluid Flow*, vol. 30, no. 5, pp. 2501–2516, 2019.
[23] M. Kothandapani, V. Pushparaj, and J. Prakash, "Effect of magnetic field on peristaltic flow of a fourth grade fluid in a tapered asymmetric channel," *Journal of King Saud University --Engineering Sciences*, vol. 30, no. 1, pp. 86–95, 2018.

[24] M. M. Bhatti, A. Zeeshan, D. Tripathi, and R. Ellahi, "Thermally developed peristaltic propulsion of magnetic solid particles in Biorheological fluids," *Indian Journal of Physics*, vol. 92, no. 4, pp. 423–430, 2018.
[25] A. Riaz, A. Zeeshan, S. Ahmad, A. Razaq, and M. Zubair, "Effects of external magnetic field on Non-Newtonian two phase fluid in an annulus with peristaltic pumping," *Journal of Magnetics*, vol. 24, pp. 62–69, 2019.
[26] S. U. Choi, "Enhancing thermal conductivity of fluid with nanoparticles developments and Applications of non-Newtonian Flow," *ASME FED*, vol. 66, no. 231, pp. 99–105, 1995.
[27] S. Akram, "Nanofluid effects on peristaltic transport of a fourth grade fluid in the occurrence of inclined magnetic field," *Scientia Iranica*, vol. 23, no. 3, pp. 1502–1516, 2016.
[28] S. Nadeem, A. Riaz, R. Ellahi, and N. S. Akbar, "Mathematical model for the peristaltic flow of Jeffrey fluid with nanoparticles phenomenon through a rectangular duct," *Applied Nanoscience*, vol. 4, no. 5, pp. 613–624, 2014.
[29] K. S. Mekheimer, W. M. Hasona, R. E. Abo-Elkhair, and A. Z. Zaher, "Peristaltic blood flow with gold nanoparticles as a third grade nanofluid in catheter: application of cancer therapy," *Physics Letters A*, vol. 382, no. 2-3, pp. 85–93, 2018.
[30] R. Ellahi, A. Zeeshan, F. Hussain, and A. Asadollahi, "Peristaltic blood flow of couple stress fluid suspended with nanoparticles under the influence of chemical reaction and activation energy," *Symmetry*, vol. 11, no. 2, p. 276, 2019.
[31] N. S. Khan, Q. Shah, A. Sohail et al., "Rotating flow assessment of magnetized mixture fluid suspended with hybrid nanoparticles and chemical reactions of species," *Scientific Reports*, vol. 11, no. 1, Article ID 11277, 2021.
[32] N. S. Khan, A. H. Usman, A. Kaewkhao, P. Kumam, P. Thounthong, and U. W. Humphries, "Exploring the nanomechanical concepts of development through recent updates in magnetically guided system," *Scientific Reports*, vol. 11, no. 1, Article ID 13576, 2021.
[33] N. S. Khan, P. Kumam, and P. Thounthong, "Magnetic field promoted irreversible process of water based nanocomposites with heat and mass transfer flow," *Scientific Reports*, vol. 11, no. 1, p. 1692, 2021.
[34] N. S. Khan and Q. Shah, "Arif Sohail, Dynamics with Cattaneo--Christov heat and mass flux theory of bioconvection Oldroyd-B nanofluid," *Advances in Mechanical Engineering*, vol. 12, pp. 1–20, 2020.
[35] A. H. Usman, N. S. Khan, U. W. Humphries et al., "Computational optimization for the deposition of bioconvection thin Oldroyd-B nanofluid with entropy generation," *Scientific Reports*, vol. 11, no. 1, Article ID 11641, 2021.
[36] O. A. Bég and D. Tripathi, "Mathematica simulation of peristaltic pumping with double-diffusive convection in nanofluids a bio-nanoengineering model," *Proceedings of the Institution of Mechanical Engineers - Part N: Journal of Nanoengineering and Nanosystems*, vol. 225, no. 3, pp. 99–114, 2012.
[37] H. Alolaiyan, A. Riaz, A. Razaq, N. Saleem, A. Zeeshan, and M. M. Bhatti, "Effects of double diffusion convection on Third grade nanofluid through a curved compliant peristaltic channel," *Coatings*, vol. 10, no. 2, p. 154, 2020.
[38] S. Akram, Q. Afzal, and E. H. Aly, "Half-breed effects of thermal and concentration convection of peristaltic pseudoplastic nanofluid in a tapered channel with induced magnetic field," *Case Studies in Thermal Engineering*, vol. 22, Article ID 100775, 2020.
[39] S. Akram and Q. Afzal, "Effects of thermal and concentration convection and induced magnetic field on peristaltic flow of Williamson nanofluid in inclined uniform channel," *The European Physical Journal Plus*, vol. 135, no. 10, p. 857, 2020.
[40] N. S. Akbar, "Peristaltic flow of a Sutterby nanofluid with double-diffusive natural convection," *Journal of Computational and Theoretical Nanoscience*, vol. 12, no. 8, pp. 1546–1552, 2015.
[41] S. K. Asha and G. Sunitha, "Thermal radiation and hall effects on peristaltic blood flow with double diffusion in the presence of nanoparticles," *Case Studies in Thermal Engineering*, vol. 17, Article ID 100560, 2020.
[42] A. Sharma, D. Tripathi, R. K. Sharma, and A. K. Tiwari, "Analysis of double diffusive convection in electroosmosis regulated peristaltic transport of nanofluids," *Physica A: Statistical Mechanics and Its Applications*, vol. 535, Article ID 122148, 2019.
[43] W. K. H. Chu and J. Fang, "Peristaltic transport in a slip flow," *The European Physical Journal B*, vol. 16, no. 3, pp. 543–547, 2000.
[44] N. S. Akbar, S. Nadeem, T. Hayat, and A. A. Hendi, "Peristaltic flow of a nanofluid with slip effects," *Meccanica*, vol. 47, no. 5, pp. 1283–1294, 2012.
[45] F. M. Abbasi, T. Hayat, and F. Alsaadi, "Hydromagnetic peristaltic transport of water-based nanofluids with slip effects through an asymmetric channel," *International Journal of Modern Physics B*, vol. 29, no. 21, Article ID 1550151, 2015.
[46] S. Akram, A. Razia, and F. Afzal, "Effects of velocity second slip model and induced magnetic field on peristaltic transport of non-Newtonian fluid in the presence of double-diffusivity convection in nanofluids," *Archive of Applied Mechanics*, vol. 90, no. 7, pp. 1583–1603, 2020.
[47] R. Ellahi, F. Hussain, F. Ishtiaq, and A. Hussain, "Peristaltic transport of Jeffrey fluid in a rectangular duct through a porous medium under the effect of partial slip: an application to upgrade industrial sieves/filters," *Pramana*, vol. 93, no. 3, p. 34, 2019.
[48] S. Akram and S. Nadeem, "Significance of nanofluid and partial slip on the peristaltic transport of a non-Newtonian fluid with different wave forms," *IEEE Transactions on Nanotechnology*, vol. 13, no. 2, pp. 375–385, 2014.
[49] J. Prakash, E. P. Siva, D. Tripathi, and O. A. Beg, "Thermal slip and radiative heat transfer effects on electroosmotic magneto nanoliquid peristaltic propulsion through a microchannel," *Heat Transfer - Asian Research*, vol. 48, no. 7, pp. 2882–2908, 2019.
[50] A. Riaz, S. U. D. Khan, A. Zeeshan, S. U. Khan, M. Hassan, and T. Muhammad, "Thermal analysis of peristaltic flow of nanosized particles within a curved channel with second-order partial slip and porous medium," *Journal of Thermal Analysis and Calorimetry*, vol. 143, no. 3, pp. 1997–2009, 2020.